(Sub)Surface Mobility of Oxygen Vacancies at the TiO_2 Anatase (101) Surface

Philipp Scheiber,[1] Martin Fidler,[1] Olga Dulub,[2] Michael Schmid,[1] Ulrike Diebold,[1,2,*] Weiyi Hou,[3] Ulrich Aschauer,[3] and Annabella Selloni[3]

[1]*Institute of Applied Physics, Vienna University of Technology, Wiedner Hauptstrasse 8-10/134, 1040 Vienna, Austria*
[2]*Department of Physics, Tulane University, New Orleans, Louisiana 70118, USA*
[3]*Department of Chemistry, Princeton University, Frick Laboratory, Princeton New Jersey 08544, USA*

(Received 12 July 2012; revised manuscript received 16 August 2012; published 28 September 2012)

Anatase is a metastable polymorph of TiO_2. In contrast to the more widely studied TiO_2 rutile, O vacancies (V_O's) are not stable at the anatase (101) surface. Low-temperature STM shows that surface V_O's, created by electron bombardment at 105 K, start migrating to subsurface sites at temperatures $\geq$ 200 K. After an initial decrease of the V_O density, a temperature-dependent dynamic equilibrium is established where V_O's move to subsurface sites and back again, as seen in time-lapse STM images. We estimate that activation energies for subsurface migration lie between 0.6 and 1.2 eV; in comparison, density functional theory calculations predict a barrier of ca. 0.75 eV. The wide scatter of the experimental values might be attributed to inhomogeneously distributed subsurface defects in the reduced sample.

DOI: 10.1103/PhysRevLett.109.136103 PACS numbers: 68.37.Ef, 61.72.Cc, 68.35.Dv, 68.47.Gh

Titanium dioxide, TiO_2, is one of the most versatile oxide materials and finds wide use, e.g., in energy-related applications such as (photo-)catalysis and solar energy conversion schemes. TiO_2 has also evolved as a popular model system for studying the fundamentals of defect-related surface processes at the molecular scale [1,2].

TiO_2 crystallizes in three different structures commonly named rutile ($D_{4h}^{14} - P4_2/mnm$), anatase ($D_{4h}^{19} - I4_1/amd$), and brookite ($D_{2h}^{15} - Pbca$). TiO_2 nanomaterials can be synthesized with various shapes and functionalities using solgel and other processing techniques [3]. Although the anatase polymorph is metastable, it is commonly found in nanomaterials where the crystal size is below a few tens of nm. Yet few experimental studies on large single crystals exist [4–8]; thus, the surfaces of anatase are not as well understood as those of rutile, where processes related to intrinsic defects—Ti interstitials (Ti_{int}) and surface O vacancies (V_O)—have received considerable attention [9–12].

Recently, we found a significant difference between the surfaces of rutile and anatase: at anatase (101), the most stable surface of this polymorph, it is energetically more favorable for O vacancies to reside in the bulk than on the surface [13]. This is in stark contrast to rutile (110), where surface V_O's form easily under standard preparation conditions [1]. The preponderance of bulk defects in anatase was first predicted by density functional theory (DFT) calculations, which showed that the formation energy of a surface V_O is larger than that of a bulk vacancy by about 0.5 eV [14,15]. In a previous STM study [13], we compared a freshly cleaved, pristine anatase (101) sample with a more O-deficient, reduced one. STM images of the reduced anatase (101) surface have an inhomogeneous appearance that strongly depends on the STM tunneling parameters; we attributed this to a variation of the local electronic structure due to subsurface defects, i.e., O vacancies and/or Ti interstitials. We also found that more reduced anatase is more reactive towards water adsorption, despite the fact that no V_O's are visible at the surface [16].

The observation that surface V_O's are less stable than bulk V_O's is remarkable. An O atom can leave a solid only through its surface; thus, an as-formed surface V_O should diffuse into the bulk. The activation energy (E_{act}) for surface-to-subsurface migration is ~0.7 eV according to our DFT calculations. Such surface-to-bulk migration should thus be observable at temperatures that are conveniently accessible in an STM experiment; this work presents such a study. We create surface V_O's nonthermally by electron bombardment [17] and monitor their fate with low-temperature and variable-temperature STM. We find that surface V_O's diffuse to subsurface sites at temperatures above 200 K. Time-lapse STM images show a temperature-dependent, dynamic equilibrium concentration of surface defects. The results point towards an activation energy for subsurface migration of a V_O that depends on its immediate surroundings.

The experiments were carried out in a two-chamber UHV system with a base pressure of 10^{-11} mbar. Unless noted otherwise, constant-current STM measurements were performed at 78 K. We typically used positive sample bias voltages between 1.3 and 1.5 V and tunneling currents between 0.1 and 0.4 nA for STM. A mineral anatase (101) sample was cleaved *ex situ* as described in Ref. [18]. A clean, almost pristine surface was repeatedly prepared by sputtering (1 keV Ar^+, fluence of 7×10^{15} ions/cm^2), annealing in O_2 ($p = 5 \times 10^{-7}$ mbar) at 923 K for 30 min, and postannealing in UHV at 973 K for another 10 min; see Fig. 1(a). To create V_O's, the surface was irradiated with electrons from a thoroughly outgassed, rastered electron gun (500 eV, current density of 8 μA cm^{-2}, measured with a positive sample bias of 27 V). Electron bombardment was performed in the preparation chamber

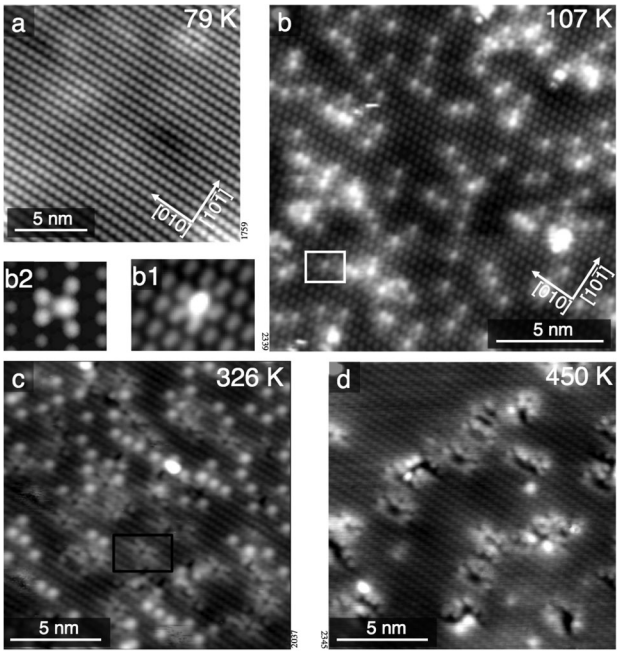

FIG. 1. STM images ($T_{\text{sample}} = 78$ K) of TiO_2 anatase (101). (a) Freshly prepared surface. (b) After irradiation with 500 eV electrons, which creates surface O vacancies (V_O's). The insets (b1) and (b2) show a magnified experimental and calculated STM image of a V_O, respectively. Images obtained after annealing the sample for 10 min to (c) 326 K and (d) 450 K.

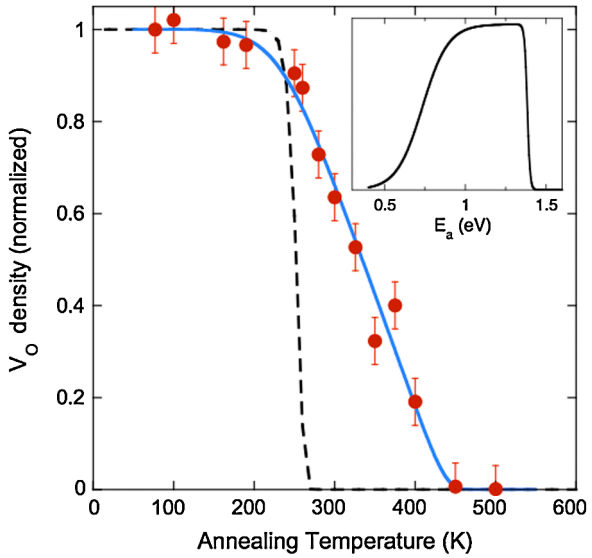

FIG. 2 (color online). Stability of surface V_O's created by electron beam bombardment. The plot shows the density of V_O's after heating the sample to various temperatures for 10 min, normalized to the initial value after electron irradiation at 105 K. The dashed line shows the expected behavior assuming one E_{act} of 0.75 eV. The solid line assumes the trapezoidal distribution of E_{act}'s from 0.6 to 1.2 eV displayed in the inset.

with the sample kept at 105 K. As shown below, V_O's are immobile at this temperature. After irradiation, the sample was transferred into the STM instrument for analysis. To determine the temperature stability of the electron-induced surface defects (Fig. 2), we proceeded as follows: The manipulator in the preparation chamber was resistively heated and equilibrated at the desired temperature. With a precooled wobblestick, the sample was taken from the cold STM instrument and inserted into the manipulator, where it was kept for 10 min. Then the sample was transferred back into the cold STM. The minimum time between taking the sample from the manipulator and the first usable STM image was also 10 min. It is important to note (see below) that the initial V_O density was kept constant throughout these experiments.

The DFT calculations were performed using the Perdew–Burke–Ernzerhof (PBE) [19] functional and the plane wave pseudopotential scheme as implemented in the QUANTUM ESPRESSO package [20]. In addition, selected spin polarized hybrid PBE0 calculations [21] were performed using a mixed localized + plane wave basis set expansion of the electronic states as implemented in CP2KQUICKSTEP [22]. The defected surface was modeled using 3×1 (10.26×11.31 Å^2) supercells with periodically repeated slabs of three (9.7 Å) or four (13.1 Å) TiO_2layers separated by a vacuum of about 10 Å. For STM calculations, larger 4×2 (20.49×15.06 Å^2) supercells were used to separate the periodic images. Activation energy barriers were estimated using the nudged elastic band [23,24] method. Other computational details are given in the Supplemental Material [25].

The sputtered and annealed anatase (101) surface is characterized by trapezoidal islands; their orientation indicates the crystallographic directions of the crystal [26]. Atomically resolved STM shows rows of oval-shaped spots that extend over both the Ti_{5c} and O_{2c} surface atoms [5] oriented along the [010] direction [see Fig. 1(a)]. Our sample preparation procedure renders a bulk-reduced sample, as evidenced by a small shoulder in the XPS Ti $2p$ core levels. The surface has a nonuniform appearance in STM, with a long-range corrugation that depends strongly on the tunneling conditions as observed previously [13]; these are attributed to either intrinsic or extrinsic subsurface defects.

TiO_2 is sensitive to electron irradiation, which can be used to create vacancies at the undercoordinated O sites of the surface [17,27]. An STM image of an electron-irradiated anatase (101) surface is shown in Fig. 1(b). V_O's appear as extra bright features at regular lattice sites, consistent with STM simulations; see insets (b1) and (b2) of Fig. 1. After exposure to 2×10^{16} e/cm^2, the density of such V_O's amounts to 8% of a monolayer (ML, where 1 ML is defined as the number of primitive unit cells, i.e., 5.16×10^{14} cm^{-2}). Assuming a simple, first-order desorption process, we estimate a cross section for electron-induced O desorption of 4×10^{-18} cm^2.

The stability of these surface vacancies was probed by annealing the electron-irradiated sample for 10 min as described above. Each heating excursion was performed

with a freshly prepared and irradiated surface; the V_O densities after the annealing steps are shown in Fig. 2. No significant change was observed up to a temperature of 200 K; after an anneal to 230 K, the defect density decreases significantly. The higher the sample temperature during the 10 min anneal, the fewer V_O's survive. Above 320 K, new features appear that span several unit cells; one is marked with a black box in Fig. 1(c). These features (not taken into account in Fig. 2) become more extended when an electron-irradiated surface is heated to higher temperatures [Fig. 1(d)] and disappear completely above 500 K.

In addition to heating excursions, we also followed the fate of single V_O's in time-lapse images at various temperatures. For these measurements we first equilibrated the STM for several hours at a specific temperature between 220 and 300 K. Electron bombardment of the freshly prepared sample was again performed at 105 K. (At this temperature we do not expect any surface-to-bulk migration, Fig. 2.) The irradiated sample was inserted into the temperature-stabilized STM, and series of images were taken. Figure 3(a) shows an example of such a time-lapse sequence, taken at $T_{\text{sample}} = 259$ K. One of the defects, marked with an arrow, disappears and returns to the same spot a few frames later. We also observed that defects disappeared at one position and appeared at another position at the same or—less frequently—a neighboring row. The mobility of V_O's increases with temperature; see Fig. 3(c). The total defect density, however, remains constant within the time frame of the experiment; see Fig. 3(b).

It takes at least 10 min between the end of electron-irradiation (at 105 K) and the recording of the time-lapse sequences in our experimental setup. During this time the total defect density decreases significantly, as shown in Fig. 2. This is the reason why the absolute V_O densities in Fig. 3 vary with temperature. On the other hand, the fact that the number of defects stays constant [Fig. 3(b)] after the original, rapid decrease gives us confidence that the data displayed in Fig. 2 indeed show the equilibrium concentrations at the given temperatures and that the finite time constants of our experiment do not influence the results.

By DFT calculations, we estimate that the barrier, E_{act}, for surface-to-bulk migration of V_O's is 0.75 eV, whereas it is 1.15 eV for the reverse process (slight differences with respect to the barriers in Ref. [15] are due to the larger surface model used for the present nudged elastic band calculations). The dashed line in Fig. 2 shows the expected behavior if we adapt this E_{act} and a conventionally used prefactor of 10^{12} s^{-1}. While the onset of bulk migration is consistent with the DFT result, the expected decrease with temperature is much steeper than the measured one. In addition, the disappearance or reappearance of the surface V_O's, which leads to a temperature-dependent dynamic equilibrium, is hard to reconcile with the picture derived from our DFT calculations: once the sample temperature is high enough to overcome the energetic barrier for surface-to-bulk migration,

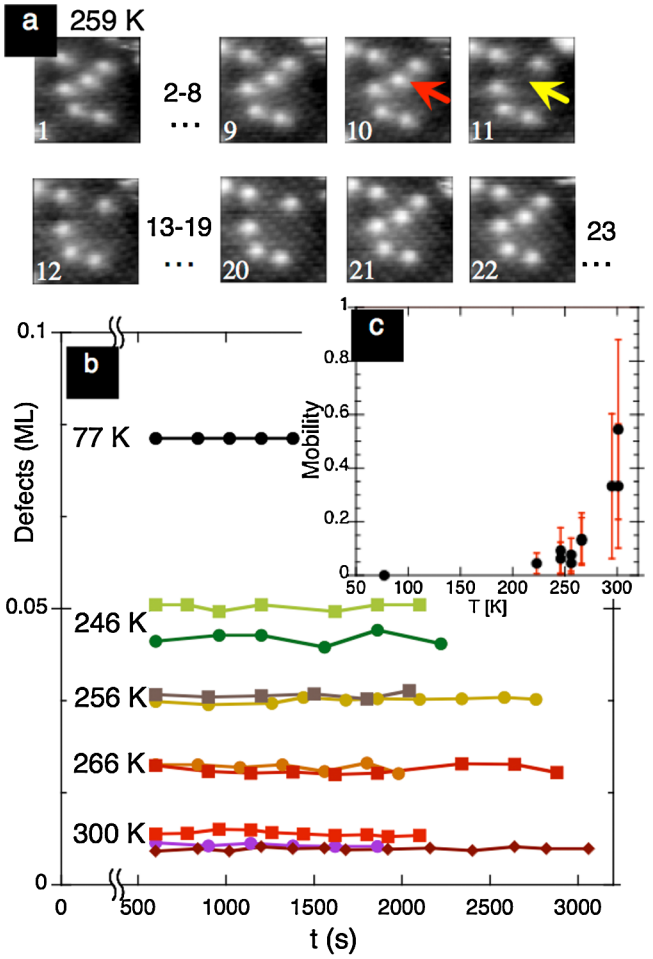

FIG. 3 (color online). (Color online) Results from time-lapse STM images of surface V_O's on anatase (101). (a) Series of images (4×4 nm^2; +1.6 V/0.2 nA) recorded at $T = 259$ K; the time between images was 3.2 min. The arrows mark a V_O that disappears and reappears at the same position. (b) Total defect density in time-lapse images; each trace corresponds to a separate experimental run at the sample temperature indicated. (c) Defect mobility, represented by the number of hopping events per defect and frame for different temperatures.

there is little reason for a V_O to return back to the surface. One should consider, however, that the calculations were performed assuming an idealized case, i.e., a perfect anatase slab devoid of any other defects except the single V_O under investigation. This is different from the situation in the experiment, where subsurface defects are present at the outset. From titration experiments using O_2 adsorption we estimate that the density of Ti_{int}'s and V_O's in the near-surface region of our sample amounts to 2 ($\pm$ 1)% of a ML at the clean, as-prepared surface. The uneven appearance of the STM images from the clean surface [Fig. 1(a)] is attributed to local band bending effects. Thus, at least some of the subsurface defects are charged; plausibly these exert a considerable influence on the energetics and dynamics of defects migrating within their neighborhood. It is not unreasonable to assume a range of E_{act}'s for subsurface diffusion, as this value will depend on

the immediate environment of each surface V_O. The solid line in Fig. 2 takes into account such a scenario, where we assume a trapezoidal distribution of E_{act}'s ranging from 0.6 to 1.2 eV, as displayed in the inset of Fig. 2.

The time- and temperature-dependent behavior of V_O's can also be explained with such a range of activation energies: starting with a certain surface V_O concentration, the defects that happen to reside above a relatively perfect region of the sample can disappear into the bulk once a temperature >200 K is reached. If another defect is present within the selvedge of the crystal, it will affect the V_O and change the activation energy for its disappearance into the bulk. It is well possible that the defect migrates a certain distance in the subsurface region before it pops up again—estimates for lateral diffusion energies are in the range of 1.1–1.8 eV (see Supplemental Material [25]); hence, the V_O's can appear at different positions, as is observed in the experiment. The extended features observed in Figs. 1(c) and 1(d) suggest that V_O's aggregate in the near-surface region at moderate annealing temperatures. The temperature dependence of bulk diffusion and defect equilibria observed in this work are possibly affected by the initial V_O concentration; this could be tested in future experiments.

The experimental results presented in this work are unequivocal proof for the theoretical prediction that vacancies are more stable in the bulk than at the surface. This prediction, originally based on DFT-PBE calculations [14,15], is also supported by results from hybrid calculations which account for the polaronic character of V_O-induced Ti^{3+} states and are thus considered more accurate for the study of defects in TiO_2 [28,29]; see Supplemental Material [25]. While hybrid calculations are still too demanding to be used for diffusion barrier determinations, DFT + U studies indicate that the barriers for the hopping diffusion of the Ti^{3+} polarons are low, typically between 0.1 and 0.3 eV [30–32]. Therefore, the effect of excess electron localization on V_O migration barriers is expected to be relatively minor, as has recently been shown for H diffusion in anatase [33].

An inspection of the anatase (101) surface structure provides a simple qualitative rationale for the instability of surface V_O's: removal of an O_{2c} gives rise to one fivefold and one highly unstable fourfold coordinated Ti^{3+} cation, whereas the Ti^{3+} cations neighboring bulk V_O's are fivefold coordinated. Moreover, the Ti–O_{2c} bonds are short and strong, so breaking two Ti–O_{2c} bonds at the surface is energetically more costly than breaking three in the bulk. Clearly, the resulting subsurface defects have to be reckoned with when considering the surface chemistry of TiO_2 anatase, and some observations have already been interpreted along these lines [16,34]. Subsurface migration automatically results in inhomogeneity within the selvedge of the crystal, which in turn affects the activation energies. The dynamic equilibrium of surface O vacancies will then depend on the presence of intrinsic as well as extrinsic charged defects. Even at room temperature defects come and go from the surface, suggesting that the chemically active sites change across the surface.

Generally, the flow of lattice oxygen (defects) to and from the surface is of continued interest in solid-state chemistry and important in established and emerging technologies such as catalysis [35], solid-oxide fuel cells [36], and memristor devices [37]. Direct observation of such defect migration, combined with modeling at the atomic scale, can help pave the way for future experiments that give insights into the relevant processes.

This work was supported by the Austrian Science Fund (FWF; Project F45) and the ERC Advanced Grant "OxideSurfaces." A. S. acknowledges support from DOE-BES, Chemical Sciences, Geosciences and Biosciences Division under Contract No. DE-FG02-12ER16286. Calculations were performed at the TIGRESS high-performance computer center at Princeton University.

*diebold@iap.tuwien.ac.at

[1] U. Diebold, Surf. Sci. Rep. **48**, 53 (2003).
[2] C. L. Pang, R. Lindsay, and G. Thornton, Chem. Soc. Rev. **37**, 2328 (2008).
[3] X. Chen and S. Mao, Chem. Rev. **107**, 2891 (2007).
[4] U. Diebold, N. Ruzycki, G. Herman, and A. Selloni, Catal. Today **85**, 93 (2003).
[5] W. Hebenstreit, N. Ruzycki, G. S. Herman, Y. Gao, and U. Diebold, Phys. Rev. B **62**, R16334 (2000).
[6] N. Ruzycki, G. Herman, L. Boatner, and U. Diebold, Surf. Sci. **529**, L239 (2003).
[7] M. Xu, Y. Gao, E. M. Moreno, M. Kunst, M. Muhler, Y. Wang, H. Idriss, and C. Wöll, Phys. Rev. Lett. **106**, 138302 (2011).
[8] L. Walle, A. Borg, E. M. J. Johansson, S. Plogmaker, H. Rensmo, P. Uvdal, and A. Sandell, J. Phys. Chem. C **115**, 9545 (2011).
[9] Z. Dohnálek, I. Lyubinetsky, and R. Rousseau, Prog. Surf. Sci. **85**, 161 (2010).
[10] S. Wendt, P. T. Sprunger, E. Lira, G. K. H. Madsen, Z. Li, J. O. Hansen, J. Matthiesen, A. Blekinge-Rasmussen, E. Laegsgaard, and B. Hammer *et al.*, Science **320**, 1755 (2008).
[11] C. M. Yim, C. L. Pang, and G. Thornton, Phys. Rev. Lett. **104**, 036806 (2010).
[12] Z. Zhang and J. T. Yates, Jr., J. Phys. Chem. C **114**, 3098 (2010).
[13] Y. He, O. Dulub, H. Cheng, A. Selloni, and U. Diebold, Phys. Rev. Lett. **102**, 106105 (2009).
[14] H. Cheng and A. Selloni, J. Chem. Phys. **131**, 054703 (2009).
[15] H. Cheng and A. Selloni, Phys. Rev. B **79**, 092101 (2009).
[16] U. Aschauer, Y. He, H. Cheng, S. Li, U. Diebold, and A. Selloni, J. Phys. Chem. C **114**, 1278 (2010).
[17] O. Dulub, M. Batzill, S. Solovev, E. Loginova, A. Alchagirov, T. E. Madey, and U. Diebold, Science **317**, 1052 (2007).

[18] O. Dulub and U. Diebold, J. Phys. Condens. Matter **22**, 084014 (2010).
[19] J. P. Perdew, K. Burke, and M. Ernzerhof, Phys. Rev. Lett. **78**, 1396 (1997).
[20] P. Giannozzi, S. Baroni, N. Bonini, M. Calandra, R. Car, C. Cavazzoni, D. Ceresoli, G. L. Chiarotti, M. Cococcioni, and I. Dabo *et al.*, J. Phys. Condens. Matter **21**, 395502 (2009).
[21] J. P. Perdew, M. Ernzerhof, and K. Burke, J. Chem. Phys. **105**, 9982 (1996).
[22] J.VandeVondele, M. Krack, F. Mohamed, M. Parrinello, T. Chassaing, and J. Hutter, Comput. Phys. Commun. **167**, 103 (2005).
[23] G. Henkelman, B. P. Uberuaga, and H. Jónsson, J. Chem. Phys. **113**, 9901 (2000).
[24] G. Mills and H. Jónsson, Phys. Rev. Lett. **72**, 1124 (1994).
[25] See Supplemental Material at http://link.aps.org/supplemental/10.1103/PhysRevLett.109.136103 for computational details, minimum energy diffusion pathways of oxygen vacancies, and results of hybrid functional calculations.
[26] X. Gong, A. Selloni, M. Batzill, and U. Diebold, Nature Mater. **5**, 665 (2006).
[27] C. Pang, O. Bikondoa, D. Humphrey, A. Papageorgiou, G. Cabailh, R. Ithnin, Q. Chen, C. Muryn, H. Onishi, and G. Thornton, Nanotechnology **17**, 5397 (2006).
[28] M. Ganduglia-Pirovano, A. Hofmann, and J. Sauer, Surf. Sci. Rep. **62**, 219 (2007).
[29] E. Finazzi, C. Di Valentin, G. Pacchioni, and A. Selloni, J. Chem. Phys. **129**, 154113 (2008).
[30] N. A. Deskins and M. Dupuis, Phys. Rev. B **75**, 195212 (2007).
[31] P. M. Kowalski, M. F. Camellone, N. N. Nair, B. Meyer, and D. Marx, Phys. Rev. Lett. **105**, 146405 (2010).
[32] N. A. Deskins, R. Rousseau, and M. Dupuis, J. Phys. Chem. C **115**, 7562 (2011).
[33] U. Aschauer and A.Selloni, Phys. Chem. Chem. Phys. (in press).
[34] M. Xu, H. Noei, M. Buchholz, M. Muhler, C. Wöll, and Y. Wang, Catal. Today **182**, 12 (2012).
[35] F. Esch, S. Fabris, L. Zhou, T. Montini, C. Africh, P. Fornasiero, G. Comelli, and R. Rosei, Science **309**, 752 (2005).
[36] J. Suntivich, H. A. Gasteiger, N. Yabuuchi, H. Nakanishi, J. B. Goodenough, and Y. Shao-Horn, Nature Chem. **3**, 546 (2011).
[37] R. Waser and M. Aono, Nature Mater. **6**, 833 (2007).